

# Tau lepton reconstruction at collider experiments using impact parameters

Daniel Jeans

*Department of Physics, Graduate School of Science, The University of Tokyo.*

---

## Abstract

We present a method for the reconstruction of events containing hadronically decaying  $\tau$  leptons at collider experiments. This method relies on accurate knowledge of the  $\tau$  production vertex and precise measurement of its decay products. The method makes no assumptions about the  $\tau$  kinematics, and is insensitive to momentum loss along the beam direction. We demonstrate the method using  $e^+e^- \rightarrow \mu^+\mu^-\tau^+\tau^-$  events fully simulated in the ILD detector.

*Keywords:* tau lepton, reconstruction techniques.

---

## 1. Introduction

Studies of final states including  $\tau$  leptons are of interest at current and future collider experiments; as an example, the dominant leptonic decay of the Higgs boson is to a  $\tau$  pair. A new generation of high energy particle colliders [1, 2, 3, 4] is presently under study. A key scientific aim of these facilities is to measure the Higgs boson's properties with great precision, important aspects of which involve measurements of the  $\tau$  final state. An example is the use of measurements of the  $\tau$  spin state to probe the CP nature of the Higgs boson. The detectors being designed for use at these accelerators will be equipped with vertex detectors providing unprecedented impact parameter resolution (see *e.g.* [5]), giving rise to intriguing possibilities in the reconstruction of relatively long-lived states such as the  $\tau$  lepton.

We report on a method which uses a high-precision vertex detector together with other tracking and calorimetric detectors to fully reconstruct the kinematics of events containing hadronically decaying  $\tau$ s (*i.e.* decays in which only one  $\nu$  is produced) in an unbiased way. We outline previously used techniques for the kinematic reconstruction of single- $\nu$   $\tau$  decays in section 2. In section 3 we define a new procedure which, in certain topologies, can fully reconstruct the  $\tau$  kinematics with significantly less stringent assumptions than previous approaches. This new method is then applied to  $e^+e^- \rightarrow \mu^+\mu^-\tau^+\tau^-$  events in section 4, and we conclude in section 5.

## 2. Previous approaches to $\tau$ pair reconstruction

In the case of events containing a pair of  $\tau$  leptons each decaying to a single neutrino, the following method, which assumes knowledge of the rest-frame and invariant mass

of the  $\tau$  pair, but no knowledge about the  $\tau$  production vertex, is often used at lepton colliders (*e.g.* [6, 7]). The  $\tau$ -pair rest-frame can be assumed to be the centre-of-mass of the colliding beams (in the case of the  $e^+e^- \rightarrow \tau^+\tau^-$  process), or the frame recoiling against particles produced in conjunction with the  $\tau$  pair, as in the case  $e^+e^- \rightarrow \mu^+\mu^-\tau^+\tau^-$ . The  $\tau$  decay products are then boosted into the assumed  $\tau$  pair rest frame, in which the energy of the  $\tau$ s is defined by the assumed invariant mass of the  $\tau$  pair. The  $\tau$  mass then constrains the  $\tau$  momentum to be at a fixed angle to the momentum of its hadronic decay products, defining a cone around the hadronic momentum. The two cones in an event, one per  $\tau$ , have either 0, 1, or 2 intersections, corresponding to the possible solutions for the  $\tau$  momenta.

At hadron colliders, the unknown net momentum along the beam direction results in less available information to constrain the event kinematics. The invariant mass of  $\tau$  pairs can be partially estimated using the invariant masses of visible decay products and the missing transverse energy, or by applying the approximation that the  $\nu$  from  $\tau$  decay is collinear with the visible  $\tau$  decay products [8]. Another approach is to combine the measured momenta of visible  $\tau$  decay products with constraints on the  $\tau$  mass and global event transverse momentum balance, resulting in an under-constrained system. The likelihood of the various  $\tau$  decay topologies allowed by the constraints can then be used to choose a best solution, or alternatively to associate a weight to each solution *e.g.* [9, 10, 11].

If the  $\tau$  production vertex is precisely known, the use of the impact parameters of the charged  $\tau$  daughters (“prongs”) brings additional information. The knowledge of the production vertex can come from the reconstruction of particles recoiling against the  $\tau$ s, or from *a priori* knowledge of the interaction point, if the size of the interaction region is sufficiently smaller than the impact parameters of the  $\tau$  decay products. The use of the impact parameter vectors of charged  $\tau$  daughters, without full reconstruction of  $\tau$  decay kinematics, in the analysis of Higgs boson CP properties has been described in *e.g.* [12, 13], while their use in fully reconstructing di- $\tau$  systems of known invariant mass and momentum have been demonstrated in [14, 15].

### 3. Method

In this section we present methods that can, under certain conditions, fully reconstruct a  $\tau$  without assuming that it belongs to a  $\tau$  pair of particular invariant mass or centre-of-mass frame. In section 3.2 we consider the reconstruction of hadronic single prong final states, in which a single charged hadron is produced with zero or more neutral hadrons and a single neutrino. Such decays account for 49.5% of  $\tau$  decays. Multiprong hadronic  $\tau$  decays, in which three or more charged hadrons, zero or more neutral hadrons, and a single neutrino are produced, account for 15.3% of  $\tau$  decays, are discussed in section 3.3. Leptonic decays of the  $\tau$  (35.2%) provide significantly less measurable information about its decay kinematics due to the production of two neutrinos, and are not further considered in this paper.

The method relies on precise knowledge of the  $\tau$  production vertex and the charged prong trajectories, and on the reconstruction of any neutral hadrons produced in the decay. Constraints on the invariant mass and lifetime of each  $\tau$ , and on the overall transverse momentum in the event, are then used to determine the  $\tau$  momenta.

### 3.1. Tau production vertex

The uncertainty on the  $\tau$  production position should be small in comparison to the decay length of the  $\tau$  and the typical impact parameters of its decay products. In final states in which the  $\tau$ s are produced together with more than one prompt charged particle, the production vertex can be directly reconstructed on an event-by-event basis using the tracks of these particles (e.g. the  $\mu$ s in the process  $e^+e^- \rightarrow \mu^+\mu^-\tau^+\tau^-$ ). The proposed linear electron-positron colliders [1, 2] have rather small interaction regions, which may be used as an additional constraint on the interaction point, although this is not done for the results presented in this paper.

### 3.2. Single prong $\tau$ decays

#### 3.2.1. Tau decay plane

In the case of single prong hadronic  $\tau$  decays, the trajectory of the charged prong (helical in the usual case of a uniform magnetic field) can be used to define a plane (hereafter called the “track plane”) which contains two vectors:  $\mathbf{d}$ , the vector between the reconstructed interaction point (IP, assumed to be the  $\tau$  production vertex) and the point on the trajectory closest to the IP (point of closest approach PCA); and  $\mathbf{p}$ , the tangent to the trajectory at the PCA. In the case of linear trajectories of the  $\tau$  and of the prong between the PCA and the  $\tau$  decay vertex, the  $\tau$  momentum, and therefore also the sum of the momenta of the other decay products of the  $\tau$  (neutrinos and neutral hadrons), are constrained to lie within this plane.

The difference between the reconstructed track plane and the true  $\tau$  decay plane (defined by the  $\tau$  and prong momenta) depends on the decay length of the  $\tau$ , the accuracy with which the IP position is known, the precision of the charged prong trajectory, and the extent to which the linear approximation of the  $\tau$  and prong trajectories near the IP is valid<sup>1</sup>.

#### 3.2.2. Parameterisation of neutrino momentum

In this section we describe the parameterisation of the unmeasured neutrino momentum  $\mathbf{q}$ , based on the measured prong trajectory and neutral hadron momentum.

Neutral particles are measured as clusters in the calorimeters, or as identified conversions of photons into  $e^+e^-$  pairs within the tracker volume. The momentum to be associated to calorimeter clusters can be estimated by assigning the energy of the calorimeter cluster, a mass hypothesis (e.g. zero in the case of photon-like clusters, the  $K_L$  mass for hadronic clusters), and the direction of a straight line connecting the IP and the energy-weighted mean position of the calorimeter cluster<sup>2</sup>.

The three-momentum  $\mathbf{k}$  of the neutral hadronic system can be decomposed into components perpendicular to and within the track plane:  $\mathbf{k}_\perp$  and  $\mathbf{k}_\parallel$  respectively. Since the  $\tau$  momentum lies within the track plane, the hadronic momentum perpendicular to the

---

<sup>1</sup> The error in this linear approximation scales as the ratio of the decay length of the  $\tau$  to the radius of curvature of the prong: for a prong with  $p_T = 10$  GeV/c produced by a 50 GeV  $\tau$  of average lifetime, in a field of 3.5 T, this ratio is  $< 10^{-3}$ . An iterative approach, in which a first iteration uses the helix parameters at the PCA to the IP, while later iterations use the helix parameters at the calculated  $\tau$  decay position, should reduce any sensitivity to the prong’s curvature.

<sup>2</sup> Alternative definitions are possible: for example the line connecting a first estimate of the  $\tau$  decay position to the identified start of the calorimetric shower.

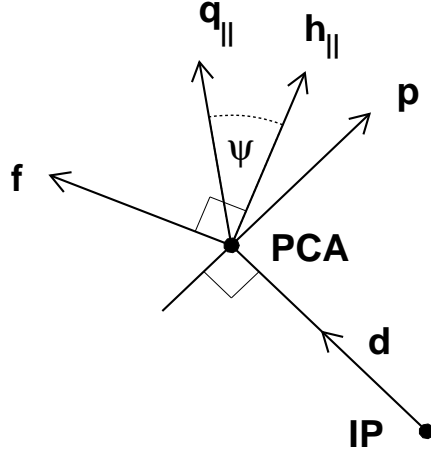


Figure 1: Parameterisation of the neutrino momentum in the track plane ( $\mathbf{q}_{\parallel}$ ) in terms of the vectors  $\mathbf{h}_{\parallel}$  and  $\mathbf{f}$ , and angle  $\psi$ . The track plane is defined by the vectors  $\mathbf{p}$  and  $\mathbf{d}$ .

track plane must be balanced by the neutrino, so the perpendicular component of the neutrino momentum  $\mathbf{q}_{\perp} = -\mathbf{k}_{\perp}$ .

The component of the neutrino momentum within the track plane can completely generally be parameterised as

$$\mathbf{q}_{\parallel} = Q \cdot (\cos \psi \cdot \hat{\mathbf{h}}_{\parallel} + \sin \psi \cdot \hat{\mathbf{f}}), \quad ^3 \quad (1)$$

where  $Q$  is the unknown magnitude of the in-plane component of the neutrino momentum,  $\mathbf{h}_{\parallel}$  is the component of the total hadronic momentum ( $\mathbf{h} = \mathbf{p} + \mathbf{k}$ ) in the track plane, and the unit vector  $\hat{\mathbf{f}} \equiv \mathbf{f}/|\mathbf{f}|$ , where  $\mathbf{f} = \mathbf{h}_{\parallel} \times (\mathbf{d} \times \mathbf{h}_{\parallel})$ , is within the plane and perpendicular to  $\mathbf{h}_{\parallel}$ .

Four-vectors  $p$ ,  $k$ , and  $q$  corresponding to the three-momenta  $\mathbf{p}$ ,  $\mathbf{k}$ , and  $\mathbf{q}$ , can be defined by means of appropriate invariant mass assumptions. The invariant mass of the sum of four-vectors  $p$ ,  $k$ , and  $q$  must be equal to the  $\tau$  lepton mass  $m_{\tau}$ . This constraint allows us to write an equation involving  $Q$  and  $\hat{\mathbf{q}}_{\parallel}$  (which in turn depends on  $\psi$ ):

$$\begin{aligned} m_{\tau}^2 &= (q + h)^2 \\ &= (\sqrt{Q^2 + \mathbf{k}_{\perp}^2} + E_h)^2 - (Q\hat{\mathbf{q}}_{\parallel} - \mathbf{k}_{\perp} + \mathbf{h})^2 \end{aligned} \quad (2)$$

where  $E_h$  is the energy of the hadronic system. This can be used to solve for  $Q$ :

$$Q = \frac{1}{2a}(-b \pm \sqrt{b^2 - 4ac}), \quad (3)$$

---

<sup>3</sup>We define  $\hat{\mathbf{x}}$  to be a unit vector parallel to  $\mathbf{x}$ .

where

$$a = B^2 - C^2, \quad b = 2AB, \quad c = A^2 - C^2 \mathbf{k}_\perp^2, \quad (4)$$

and

$$A = m_\tau^2 - m_h^2 - 2\mathbf{h} \cdot \mathbf{k}_\perp, \quad B = 2\hat{\mathbf{q}}_\parallel \cdot (\mathbf{h} - \mathbf{k}_\perp), \quad C = 2E_h, \quad (5)$$

where  $m_h$  is the invariant mass of the hadronic system.

There are in general two solutions of  $Q$  for each choice of  $\psi$ , which are complex in unphysical regions. Such complex solutions are rejected. In the case of two real solutions, we choose to denote the one with a higher energy neutrino in the laboratory frame as the “first” solution, and the other as the “second”. The first solution at  $\psi = \alpha$  corresponds to the second solution at  $\psi = \pi + \alpha$ , and *vice versa*. Since the angle between the neutrino and hadrons is typically small in the laboratory (due to the large boost of the  $\tau$ ), it is convenient to consider the solutions separately, each in the range  $-\pi/2 < \psi < \pi/2$ .

For each real solution of  $Q$ , the corresponding  $\tau$  momentum can be calculated. In conjunction with the prong trajectory, this allows the decay length and proper decay time of the  $\tau$  to be calculated. In the simple case of  $k = 0$  (*i.e.* no neutral hadrons in the  $\tau$  decay), one solution for  $Q$  corresponds to a negative  $\tau$  decay length (the intersection of the  $\tau$  trajectory with that of the prong is on the “wrong” side of the IP), and can therefore be discarded. More generally, a likelihood  $\lambda$  that the extracted lifetime is consistent with that expected of the  $\tau$  can be expressed in terms of the measured decay length of the  $\tau$  in the laboratory  $L$ , its Lorentz boost  $(\beta, \gamma)$ , and the mean lifetime of the  $\tau$  ( $\sim 87\mu\text{m}/c$ ):  $\lambda = \exp(-L/(\beta \cdot \gamma \cdot 87\mu\text{m}))$  if  $L > 0$ , and  $\lambda = 0$  otherwise.<sup>4</sup>

### 3.2.3. Choice of $\psi$

To determine the value of  $\psi$ , additional information is required. One possible approach would be to follow a statistical approach, applying a weight to each possible solution based on the likelihood that its decay time is consistent with that expected of the well-known  $\tau$  mean lifetime, and/or that the reconstructed  $\tau$  decay kinematics follow the expected distributions. If a hypothesis is made as to the energy of the  $\tau$ , or on the invariant mass of a pair of  $\tau$ s, this can also help choose appropriate  $\psi$  solutions.

An alternative approach, followed in this paper, is to consider the environment in which the  $\tau$  has been produced. We consider the class of events in which one or more single- $\nu$  decaying  $\tau$  leptons have been produced in conjunction with zero or more well-measured particles, together with zero or more particles escaping along the beam-line (e.g. ISR photons). Examples of such processes at an electron-positron collider are two-fermion production  $e^+e^- \rightarrow \tau^+\tau^-$ , Higgs-strahlung  $e^+e^- \rightarrow HZ \rightarrow (\tau^+\tau^-)(\mu^+\mu^-)$ , and its major irreducible background  $e^+e^- \rightarrow ZZ \rightarrow (\tau^+\tau^-)(\mu^+\mu^-)$ . In such events, the overall  $p_T$  of the  $\tau$ s and other visible particles is balanced, while there may be non-zero net momentum along the beam-line due to ISR. A natural way in which to determine the  $\psi$  angles in an event (one per  $\tau$  decay) is to choose that combination which minimises the magnitude of the missing transverse momentum ( $p_T^{\text{miss}}$ ) in the event. This method has the advantage of making no assumptions about  $\tau$  kinematics or about undetected particles escaping along the beam-line – also indispensable for application at hadron

---

<sup>4</sup>A more sophisticated treatment would take measurement uncertainties into account, therefore allowing small negative decay length solutions.

collider experiments, but does require that no additional neutrinos are produced in the same event. In the case of several solutions for which  $p_T^{miss}$  is consistent with zero, the reconstructed  $\tau$  lifetimes can be used to determine the most likely one, or each solution could be weighted by a likelihood based on its lifetime and/or  $\tau$  decay kinematics.

### 3.3. Multiprong $\tau$ decays

In the case of multiprong  $\tau$  decays, the prongs can be fitted to a common vertex, whose position  $\mathbf{V}$  corresponds to the point at which the  $\tau$  lepton decayed. Together with a well-known production position  $\mathbf{P}$ , this gives an estimate of the direction of the  $\tau$  momentum, in the approximation that the  $\tau$  trajectory is linear<sup>5</sup>. The  $\tau$  momentum  $\mathbf{p}_\tau$  can be written as  $\mathbf{p}_\tau = t\hat{\mathbf{r}}$ , where  $t$  is the magnitude of the  $\tau$  momentum, and  $\mathbf{r} = \mathbf{V} - \mathbf{P}$ .

The neutrino momentum  $\mathbf{q}$  can then be written as  $\mathbf{q} = \mathbf{p}_\tau - \mathbf{h}$ , where  $\mathbf{h}$  is the measured momentum of the visible hadronic system. Defining appropriate four-vectors  $q$  and  $h$  for the neutrino and hadronic system respectively, and requiring that the invariant mass of the decay products is equal to the  $\tau$  mass  $m_\tau$ , gives

$$\begin{aligned} m_\tau^2 &= (q + h)^2 \\ &= (|\mathbf{q}| + E_h)^2 - (\mathbf{q} + \mathbf{h})^2 \\ &= (|t\hat{\mathbf{r}} - \mathbf{h}| + E_h)^2 - t^2, \end{aligned} \quad (6)$$

where  $E_h$  is the energy of the hadronic system. This can be solved for  $t$ , giving

$$t = \frac{1}{2a}(b \pm \sqrt{b^2 - 4ac}), \quad (7)$$

where

$$a = E_h^2 - (\hat{\mathbf{r}} \cdot \mathbf{h})^2, \quad b = (\hat{\mathbf{r}} \cdot \mathbf{h})(m_\tau^2 + m_h^2), \quad c = -\frac{(m_\tau^2 + m_h^2)^2}{4} + m_\tau^2 E_h^2. \quad (8)$$

There are in general two possible solutions for  $t$  which satisfy the  $m_\tau$  constraint, however they are not guaranteed to be real. The full tau decay kinematics can be calculated for each real solution, including the decay length and proper decay time of the  $\tau$ . In appropriate event topologies, the  $p_T^{miss}$  of the event can be used to choose between these two solutions, otherwise the previously introduced lifetime likelihood could be used.

Since the  $\tau$  leptons produced at high energy colliders are typically highly boosted, the opening angle of the multiprong jet is usually small. As a consequence, the precision with which the  $\tau$  decay vertex is reconstructed is significantly worse along direction of the  $\tau$  jet than along the perpendicular directions. In the example considered later in this paper, in which  $\tau$ s are produced in Higgs boson decays, the length of the major axis of the vertex position error ellipsoid is typically of order  $100\mu m$ , while the other two axes have lengths of order  $2\mu m$ .

In this case, it turns out to be better to consider the major axis of the vertex error ellipsoid as a single trajectory, and to analyse the event using the procedure developed for single prong decays in the previous section. In this way, the  $\tau$  decay plane is defined by

---

<sup>5</sup> We note that the  $\tau$  momentum direction can be directly measured for any decay mode if the  $\tau$  decay length is sufficiently large for it to produce hits in the vertex detector.

the IP and the centre and major axis of the vertex ellipsoid, and the exact decay position along the major axis direction is left as a free parameter. The distance between the fitted and reconstructed vertex positions, normalised by the uncertainty on the reconstructed vertex position, can be used to define a vertex likelihood, which can be used when choosing between several possible solutions.

#### 4. Example application

We apply this method to  $e^+e^- \rightarrow \mu^+\mu^-H$  events, in which the Higgs boson decays to a pair of  $\tau$ s. Such events are usually selected by considering the mass recoiling against the di- $\mu$  system, which has a peak at the Higgs boson mass. However the distribution of this recoil mass has a long tail due to beamstrahlung and ISR, particularly at higher centre-of-mass energies well above threshold. If the invariant mass of the  $\tau\tau$  system can be directly reconstructed, a rather cleaner selection of such events should be possible. The full reconstruction of the  $\tau$  decay kinematics and the  $\tau\tau$  centre-of-mass frame also allows the best use of the spin information of the  $\tau$ s: the properties of the  $\tau$  decays can be used to define their *polarimeter vectors*, and the correlations between the  $\tau$  polarimeters can be used to measure the CP-nature of the Higgs boson (*e.g.* [14]).

Events were generated at a centre-of-mass energy of 250 GeV using WHIZARD v2.2.2[16], assuming a Higgs boson mass of 125 GeV, and including effects due to initial state radiation and beamstrahlung (by CIRCE1). The  $\tau$ s were decayed by TAUOLA++ v1.1.4[17]. Three scenarios were considered: both  $\tau$ s decaying to  $\pi^\pm\nu$ ; both decaying to  $\pi^\pm\pi^0\nu_\tau$ ; and both decaying to  $(a_1 \rightarrow 3\pi^\pm)\nu$ . The simplest hadronic  $\tau$  decay mode is  $\pi^\pm\nu$ , but accounts for only 11.5% of  $\tau$  decays, while the  $\rho\nu$  mode has the largest branching ratio of 26.0%.<sup>6</sup>

The resulting events we passed through the GEANT4-based MOKKA simulation of the ILD\_o1\_v05 detector model [5]. This model consists of a vertex detector with three double-layers of silicon pixel detectors, a silicon strip-based inner tracker and forward tracking disks, a large time projection chamber within a silicon tracking envelope, followed by highly granular calorimeters: a silicon-tungsten ECAL and scintillator-iron HCAL. These are placed within a solenoid producing a 3.5T magnetic field, surrounded by an instrumented iron flux return yoke. The simulated energy deposits within the active detectors were passed through the standard ILD digitisation procedures to simulate detector signals.

##### 4.1. Event reconstruction

The standard ILD reconstruction software was used to reconstruct charged particle tracks and calorimeter clusters. For the results shown in this paper, the reconstructed tracks were associated to primary muons and charged pions from  $\tau$  decays on the basis of matching to the simulated particle directions. In a full analysis, muon and pion identification should be performed. This is rather simple task in detectors with highly granular calorimeters such as ILD, which should not present any great difficulties. Distributions of the impact parameter in the plane perpendicular to the beam  $d_0$ , and of its uncertainty,

---

<sup>6</sup> The vast majority of  $\tau \rightarrow \pi^\pm\pi^0\nu_\tau$  decays proceed via the  $\rho^\pm$ , so we use  $\rho\nu$  as shorthand for  $\pi^\pm\pi^0\nu_\tau$  in this paper.

are shown in fig. 2 for both prompt  $\mu$  tracks and  $\pi$  tracks from  $\tau$  decay. The two  $\mu$  tracks were fitted to a common vertex to measure the event IP using the LCFIVERTX[18] package, achieving a typical precision on the IP position of better than  $3\mu m$  in all three dimensions.

Clusters identified in the electromagnetic calorimeter by the GARLIC[19] and PANDORAPFA[20] algorithms were treated as photon candidates. Each cluster was assigned a momentum with magnitude equal to the reconstructed cluster energy and direction parallel to a line joining the nominal IP and the energy-weighted mean position of the cluster. Clusters were associated to  $\pi^0$ s and their parent  $\tau$ s based on matching the cluster momentum direction to the simulated photon directions. Events were rejected if not all the simulated  $\mu$ ,  $\pi$  and photons could be matched to reconstructed particles. Such cases are typically due to imperfect reconstruction algorithms or the interactions of particles in the tracker volume.

In order to improve the effective photon energy resolution, clusters associated to a  $\pi^0$  were subjected to a constrained kinematic fit imposing the  $\pi^0$  mass by varying their energies. No special effort was made to correct invariant mass biases occurring when reconstructing two overlapping clusters from  $\pi^0$  decay. Figure 2 shows the precision with which the visible invariant mass is reconstructed in  $\tau \rightarrow \rho\nu$  decays. The accuracy with which the reconstructed track plane approximates the true  $\tau$  decay plane is demonstrated in the bottom right plot of fig. 2, in which the “track plane error” is defined as the angle that the true  $\tau$  momentum makes to the reconstructed track plane.

The reconstructed tracks from multiprong  $\tau$  decays were fitted to a common vertex, again using the LCFIVERTX package. In three-prong decays via the  $a_1$ , the ellipsoid describing the vertex position uncertainty typically has a major axis length of  $100\mu m$ , and the other two axes around  $2\mu m$ .

#### 4.2. Dependence of $p_T^{miss}$ and the lifetime likelihood on $\psi^\pm$

Figure 3 shows the dependence of the event  $p_T^{miss}$  (defined as the magnitude of the component of  $\mathbf{P} = \sum_i \mathbf{p}_i$  transverse to the beam-line, where the index  $i$  runs over the momenta  $\mathbf{p}_i$  of the  $\tau$ s and other reconstructed particles in the event) and lifetime likelihood on the two  $\tau$  decay angles  $\psi^\pm$  in two events, one in which both  $\tau \rightarrow \pi^\pm\nu$ , the other in which both  $\tau \rightarrow \rho\nu$ . The distributions are shown for the case in which the first Q solution is used for each  $\tau$  (which is where the best solution was found in these two events). Four minima at which  $p_T^{miss} \sim 0$  are seen, one in each quadrant. The lifetime likelihood (shown for the same Q solution), together with the  $p_T^{miss}$  at the minimum, allows the best minimum to be chosen.

The MINUIT package in the ROOT[21] analysis framework was used to find the minima of the  $p_T^{miss}$  distributions separately in each of the four quadrants bounded by  $\psi^\pm = 0, \pm\pi/2$ , in each of the four Q-solution combinations. If no minimum was found, or either  $\tau$  had a negative reconstructed decay length at the minimum, the quadrant was rejected. Of the remaining possible solutions, the one with the smallest value of  $p_T^{miss}$  was chosen.

#### 4.3. Results

##### 4.3.1. Single prong decays

Of events in which reconstructed objects could be unambiguously matched to simulated particles, no good solution was found in 0.4% (2.4%) of events in the  $\pi^\pm\nu(\rho\nu)$



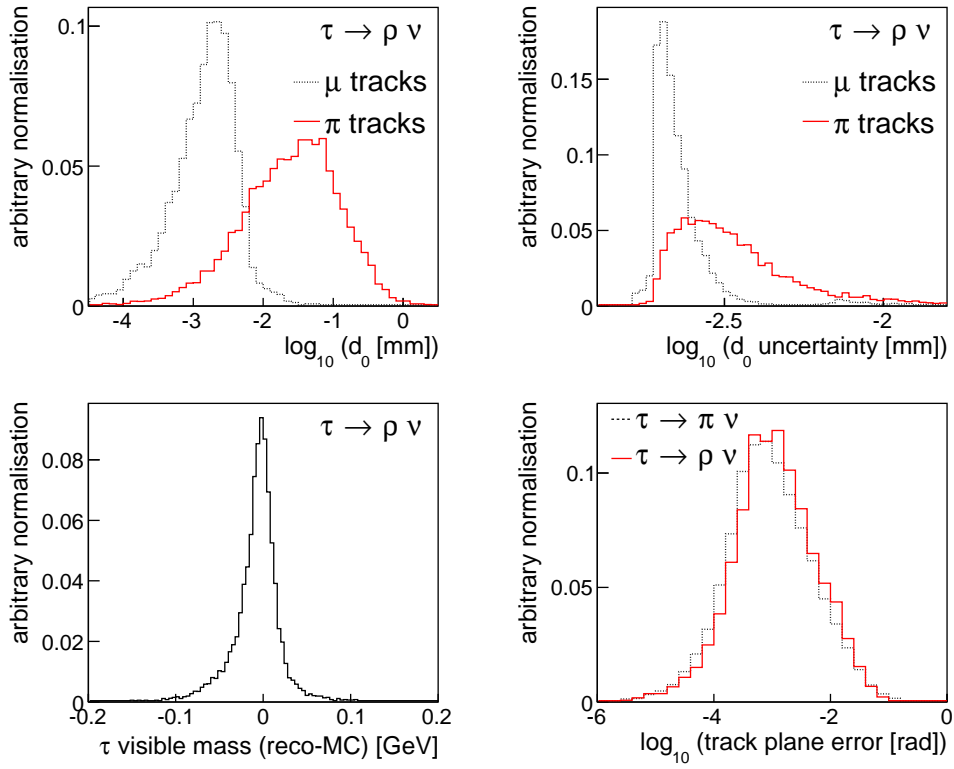


Figure 2: Properties of the considered  $e^+e^- \rightarrow \mu^+\mu^-H$  events. Top: the measured 2-d impact parameter  $d_0$  [left] and its uncertainty [right], for prompt  $\mu$  tracks, and  $\pi$  tracks from  $\tau \rightarrow \rho\nu$  decay. Bottom left: the difference between the reconstructed and true visible  $\tau$  mass in  $\tau \rightarrow \rho\nu$  decays. Bottom right: the angle between the reconstructed track plane and the true direction of the  $\tau$  momentum.

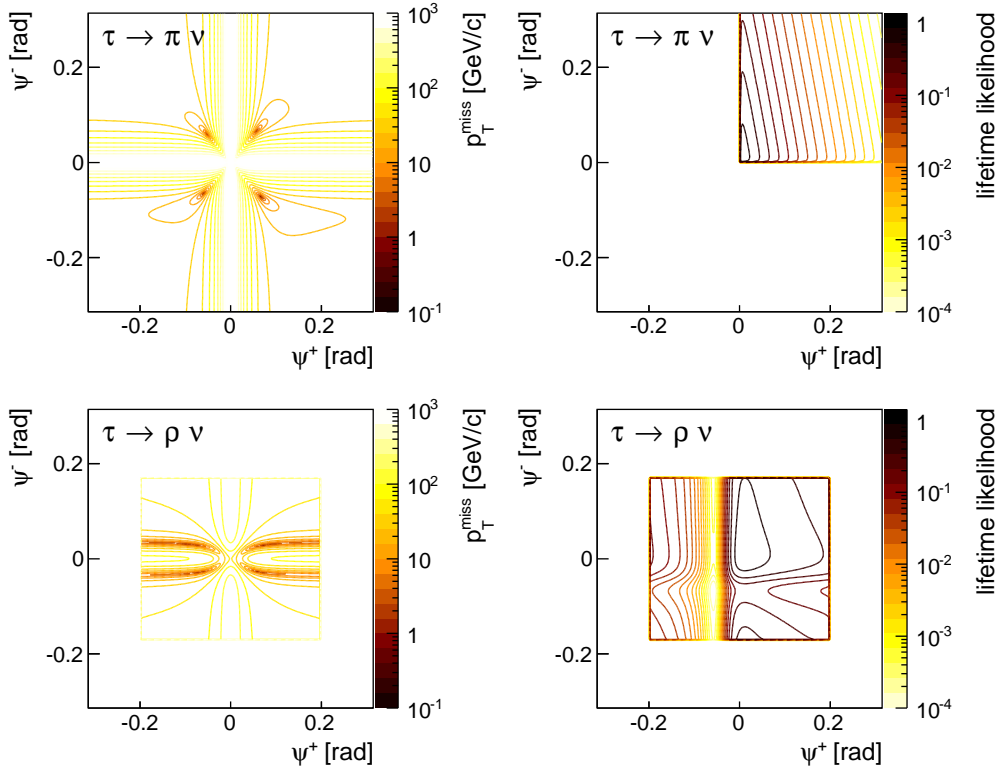


Figure 3: Example of two  $e^+e^- \rightarrow \mu^+\mu^-\tau^+\tau^-$  events in which both  $\tau \rightarrow \pi^\pm\nu$  [top], or both  $\tau \rightarrow \rho\nu$  [bottom]. Contours of  $p_T^{miss}$  [left] and lifetime likelihood [right] as a function of the two angles  $\psi^\pm$  are shown. Regions with darker contours (lower  $p_T^{miss}$ , higher lifetime likelihood) are preferred. In the upper event no positive decay length solutions were found for  $\psi^\pm < 0$ , while in the lower event, no physical solutions were found for  $|\psi^\pm| > \sim 0.2$ .

channel. This inefficiency is due to cases in which the reconstructed visible mass is larger than the  $\tau$  mass, or in which no solution with positive decay length is found. In fig. 4 we show the distribution of the chosen solutions'  $p_T^{miss}$ , for events in which both  $\tau$ s were forced to decay to either  $\pi^\pm\nu$  or  $\rho\nu$ . A rather good minimum ( $p_T^{miss} < 1$  MeV) is found in the large majority of cases, but a fraction of events have a larger  $p_T^{miss}$ . These events with large  $p_T^{miss}$  are due to mis-reconstruction of the event, and make up a larger fraction of  $\rho\nu$  than  $\pi^\pm\nu$  decays due to the relatively worse precision of the calorimeters compared to the tracker. Events in which the reconstructed  $p_T^{miss}$  is larger than around 0.5 GeV/c show a significantly wider peak in the  $\tau - \tau$  mass distribution, as shown in fig. 4. The mass distribution in the case of  $\pi^\pm\nu$  ( $\rho\nu$ ) decays has a central peak with a Gaussian width  $\sigma \sim 0.6$  GeV (1.1 GeV), and non-Gaussian tails to both higher and lower values. Of  $\pi^\pm\nu$  ( $\rho\nu$ ) events with  $p_T^{miss} < 0.5$  GeV/c, 74% (67%) lie within  $3\sigma$ , and 95% (89%) within 10 GeV, of the peak position.

The same figure also shows the reconstructed invariant mass of the two  $\tau$  system in events with small or large ISR/beamstrahlung energy (demonstrating that the method is independent of the total centre-of-mass energy and boosts along the beam-line), and on the smaller of the true  $\tau$  decay lengths in the laboratory (showing that events with longer decay lengths tend to be better reconstructed). Figure 5 shows the  $\tau$  pair mass in the  $e^+e^- \rightarrow \mu^+\mu^-H$  event sample, and a second  $e^+e^- \rightarrow \mu^+\mu^-\tau^+\tau^-$  sample in which the Higgs boson contribution was effectively turned off. Clear mass peaks due to the Higgs and  $Z^0$  bosons can be seen, the widths of which allow a rather clean separation between these processes in both the considered  $\tau$  decay modes.

#### 4.3.2. Multiprong decays

Multiprong  $\tau$  decays, studied using the  $\tau \rightarrow (a_1 \rightarrow 3\pi^\pm)\nu$  channel, are reconstructed using two methods. In the “vertex” method, the reconstructed vertex position is directly used to constrain the  $\tau$  direction, and the  $\tau$  mass constraint used to find two possible solutions for the neutrino momentum. No real solution is found in around a quarter of  $\tau$  decays. The event  $p_T^{miss}$  is used to choose the best solution.

In the “decay plane” method, the central position and major axis of the vertex position error ellipsoid are used to define the  $\tau$  decay plane, which is then used in the same way as for single prong decays. Candidate  $\tau$  solutions are required to have fitted and reconstructed  $\tau$  decay vertices in the same hemisphere. The event candidate solution with smallest  $p_T^{miss}$  is selected. When using this method, no good candidate solution was identified in around 4.5% of events. Figure 6 shows a comparison of these two multiprong methods. As well as having a much higher efficiency for identifying a solution, the “decay plane” approach results in significantly better mass resolution. The di- $\tau$  invariant mass distribution for multiprong  $a_1$  decays obtained by using the “decay plane” method are compared to other decay channels in fig. 5, showing that multiprong decays are reconstructed with a similar precision as  $\tau \rightarrow \pi^\pm\nu$  decays.

In fig.7 we compare  $\tau$  pair mass reconstruction using the methods developed in this paper with alternative approaches. The simplest is to use the invariant mass of only the visible decay products, therefore ignoring the neutrino contribution. This clearly underestimates the invariant mass, and results in a rather wide distribution. The collinear approximation assumes that the neutrinos are parallel to the visible tau decay products, and further requires the event's  $p_T$  to be balanced, allowing the neutrino energies to be estimated. The mass distribution resulting from the collinear approximation is peaked

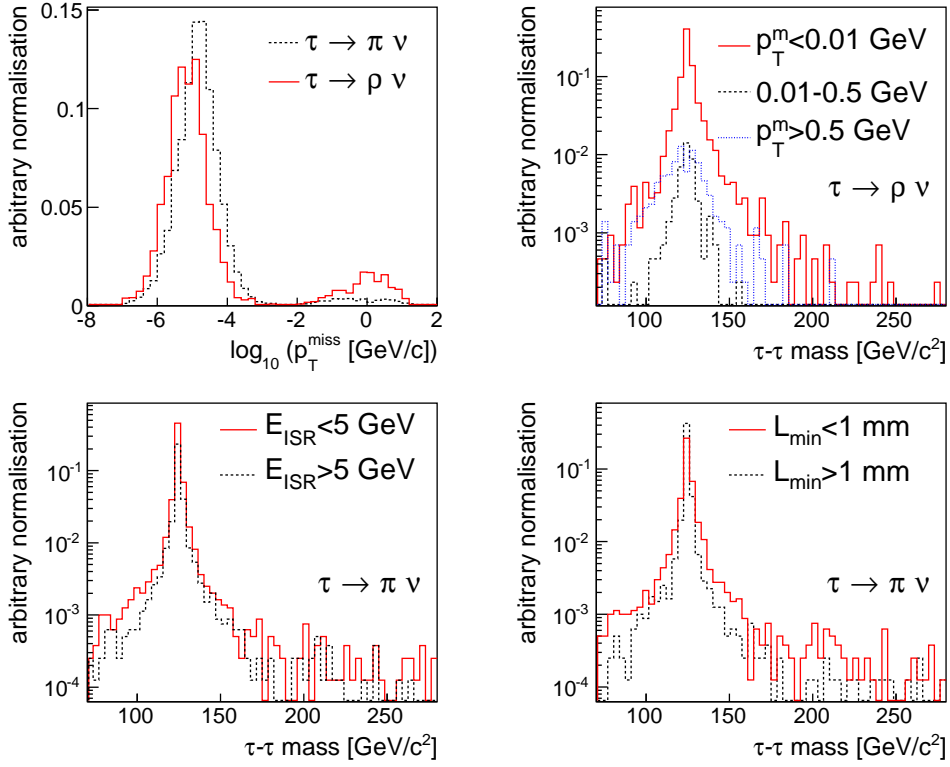


Figure 4: Properties of the considered  $e^+e^- \rightarrow \mu^+\mu^-H$  events after full  $\tau$  reconstruction. The value of the event  $p_T^{miss}$  at the chosen solution [top left]. The  $\tau$  pair mass distributions in different ranges of  $p_T^{miss}$  [top right], the total ISR/beamstrahlung energy  $E_{ISR}$  [bottom left], and  $L_{min}$ , the smaller of the two true  $\tau$  decay lengths [bottom right]. Except in the top left plot, the relative normalisations of the various contributions are as in the event samples.

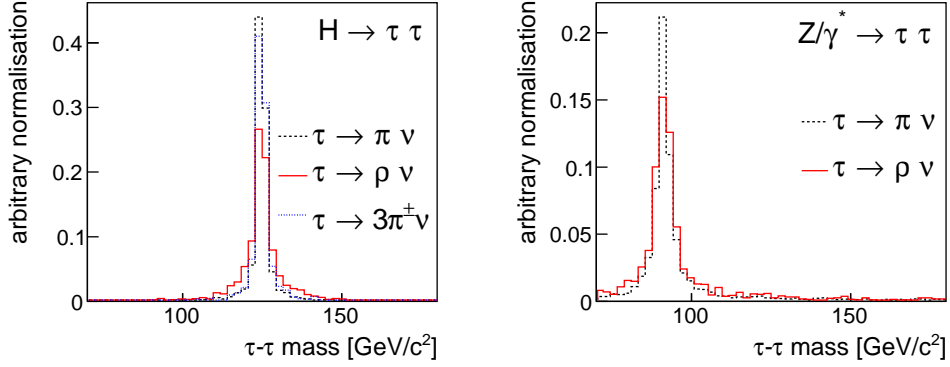


Figure 5: The reconstructed mass of the  $\tau$  pair in  $e^+e^- \rightarrow \mu^+\mu^-\tau^+\tau^-$  events in which the  $\tau$  pair was produced via a Higgs (left) or  $Z^0/\gamma^*$  (right).

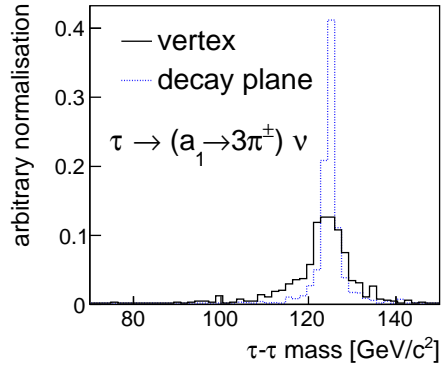


Figure 6: The reconstructed mass of the  $\tau$  pair in  $e^+e^- \rightarrow \mu^+\mu^-\tau^+\tau^-$  events in which both  $\tau$ s decay into three charged pions. We compare the results of two  $\tau$  reconstruction methods: directly using the reconstructed vertex position, and using the position and major axis of the vertex ellipsoid to define the  $\tau$  decay plane.

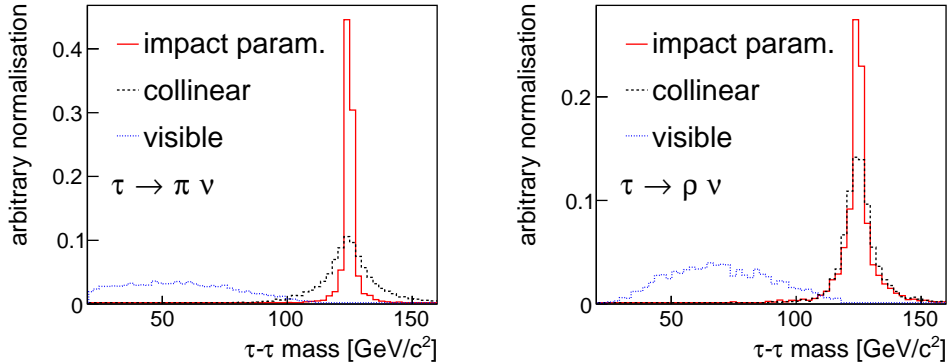


Figure 7: Comparison of the reconstructed  $\tau$  pair invariant mass using different methods: the impact parameter-based method developed in this paper, the collinear approximation, and only the visible decay products.

at the correct value, however it is significantly wider than that achieved by the methods developed in this paper. The difference in resolution is particularly significant in the  $\pi^\pm\nu$  decay channel, where the impact parameter method gives a very sharp distribution.

## 5. Conclusion

An approach to the reconstruction of hadronic  $\tau$ s has been presented, which can be used in events in which the  $\tau$  production vertex is well known, and the trajectory of its charged decay products is precisely measured. This method works only in events in which no undetected particles with significant  $p_T$  are produced together with the  $\tau$ s. In contrast to other methods, no assumptions are made on the centre-of-mass frame or the invariant mass of a  $\tau$ -pair system, nor on the  $\tau$  energies. The method is insensitive to momentum balance along the beam-line, so this method should work on *e.g.*  $e^+e^- \rightarrow \mu^+\mu^-H$  events produced both near, and well above, threshold.

The example analysed in this paper, in which a  $\tau$  pair recoils against a  $\mu$  pair, is the case in which the event  $p_T^{miss}$  is most precisely measured. The Higgs boson will more commonly recoil against a hadronic system. These events are more difficult to reconstruct, and will have a less precisely measured  $p_T^{miss}$ . The use of a constrained kinematic fit, taking into account the resolution with which the various quantities are measured, should lead to improved results.

This reconstruction technique can be used at lepton colliders, as demonstrated in this paper, provided the precision of the tracking detectors is sufficient, particularly in the estimation of charged particle trajectories near the interaction point. To be used at hadron collider experiments, the  $\tau$  decay products must be sufficiently well identified and reconstructed, and all particles produced in the same interaction unambiguously identified in order to accurately estimate the  $p_T^{miss}$  associated to the interaction. This latter point suggests that cases in which  $\tau$ s recoil against a relatively simple system, *e.g.*  $\mu - \mu$  as considered in this paper or a single high  $p_T$  jet, should be the most promising

in the richer environment of hadronic collisions at high luminosity, in which multiple interactions typically occur in each event. The method is insensitive to the unknown net momentum along the beam direction inherent in hadronic collisions.

If applied to Higgs boson decays into  $\tau$  leptons, the use of this method will allow clean separation of signal events from irreducible backgrounds from *e.g.*  $Z$  decays, and allow precise reconstruction of the  $\tau$  spin information, providing a sensitive probe to measure the CP nature of the Higgs boson.

## Acknowledgements

I thank H. Videau and S. Komamiya for helpful comments on the manuscript. This work was funded by the MEXT KAKENHI Grant-in-Aid for Scientific Research on Innovative Areas, no. 23104007.

## References

- [1] T. Behnke, et al., The International Linear Collider Technical Design Report - Volume 1: Executive Summary. [arXiv:1306.6327](#).
- [2] M. Aicheler, et al., A Multi-TeV Linear Collider Based on CLIC Technology. [doi:10.5170/CERN-2012-007](#).
- [3] A. Apyan, et al., CEPC-SPPC Preliminary Conceptual Design Report. IHEP-CEPC-DR-2015-01 (2015).
- [4] <https://fcc.web.cern.ch/> (2015).
- [5] T. Behnke, et al., The International Linear Collider Technical Design Report - Volume 4: Detectors. [arXiv:1306.6329](#).
- [6] A. Heister, et al., Measurement of the tau polarization at LEP, *Eur. Phys. J. C*20 (2001) 401–430. [arXiv:hep-ex/0104038](#).
- [7] K. Belous, et al., Measurement of the  $\tau$ -lepton lifetime at Belle, *Phys. Rev. Lett.* 112 (3) (2014) 031801. [arXiv:1310.8503](#).
- [8] R. K. Ellis, et al., Higgs Decay to tau+ tau-: A Possible Signature of Intermediate Mass Higgs Bosons at the SSC, *Nucl. Phys. B*297 (1988) 221.
- [9] A. Elagin, et al., A New Mass Reconstruction Technique for Resonances Decaying to di-tau, *Nucl. Instrum. Meth. A*654 (2011) 481–489. [arXiv:1012.4686](#).
- [10] G. Aad, et al., Evidence for the Higgs-boson Yukawa coupling to tau leptons with the ATLAS detector, *JHEP* 04 (2015) 117. [arXiv:1501.04943](#).
- [11] S. Chatrchyan, et al., Evidence for the 125 GeV Higgs boson decaying to a pair of  $\tau$  leptons, *JHEP* 05 (2014) 104. [arXiv:1401.5041](#).
- [12] K. Desch, Z. Was, M. Worek, Measuring the Higgs boson parity at a linear collider using the tau impact parameter and tau  $\rightarrow$  rho nu decay, *Eur. Phys. J. C*29 (2003) 491–496. [arXiv:hep-ph/0302046](#).
- [13] S. Berge, W. Bernreuther, Determining the CP parity of Higgs bosons at the LHC in the tau to 1-prong decay channels, *Phys. Lett. B*671 (2009) 470–476. [arXiv:0812.1910](#).
- [14] A. Rouge, CP violation in a light Higgs boson decay from tau-spin correlations at a linear collider, *Phys. Lett. B*619 (2005) 43–49. [arXiv:hep-ex/0505014](#).
- [15] M. Reinhard, CP violation in the Higgs sector with a next-generation detector at the ILC, Ph.D. thesis, LLR-École polytechnique (2009).
- [16] W. Kilian, T. Ohl, J. Reuter, WHIZARD: Simulating Multi-Particle Processes at LHC and ILC, *Eur. Phys. J. C*71 (2011) 1742. [arXiv:0708.4233](#).
- [17] N. Davidson, et al., Universal Interface of TAUOLA Technical and Physics Documentation, *Comput. Phys. Commun.* 183 (2012) 821–843. [arXiv:1002.0543](#).
- [18] D. Bailey, et al., The LCFIVertex package: vertexing, flavour tagging and vertex charge reconstruction with an ILC vertex detector, *Nucl. Instrum. Meth. A*610 (2009) 573–589. [arXiv:0908.3019](#).
- [19] D. Jeans, J. C. Brient, M. Reinhard, GARLIC: Gamma Reconstruction at a Linear Collider experiment, *JINST* 7 (2012) P06003. [arXiv:1203.0774](#).
- [20] M. Thomson, Particle Flow Calorimetry and the PandoraPFA Algorithm, *Nucl. Instrum. Meth. A*611 (2009) 25–40. [arXiv:0907.3577](#).

[21] <https://root.cern.ch> (2015).